

## ORIGINAL

# Basic study of a diagnostic modality employing a new electrical impedance tomography (EIT) method for noninvasive measurement in localized tissues

Kenji Okazaki<sup>1,6</sup>, Akira Tangoku<sup>1</sup>, Tadaoki Morimoto<sup>1,2</sup>, Ryosuke Kotani<sup>3</sup>, Keigo Hattori<sup>3</sup>, Emiko Yasuno<sup>4</sup>, Masatake Akutagawa<sup>5</sup>, and Yohsuke Kinouchi<sup>5</sup>

<sup>1</sup>Department of Thoracic, Endocrine Surgery and Oncology, Institute of Health Biosciences, the University of Tokushima Graduate School, Tokushima, Japan ; <sup>2</sup>Department of Surgery, Shikoku Central Hospital of the Mutual Aid, Ehime, Japan ; <sup>3</sup>Graduate School of Advanced Technology and Science, the University of Tokushima, Tokushima, Japan ; <sup>4</sup>Department of Systems and Control Engineering, Anan National College of Technology, Tokushima, Japan ; and <sup>5</sup>Department of Electrical and Electronic Engineering, Institute of Technology and Science, the University of Tokushima Graduate School, Tokushima, Japan

**Abstract :** The objective of this study is to develop a device for noninvasive local tissue electrical impedance tomography (EIT) using divided electrodes with guard electrodes and to validate its effectiveness using bioequivalent phantoms. For this purpose, we prepared a measurement device and bioequivalent phantoms, measured the electrical characteristics of the phantoms, and validated the method using the phantoms. Monolayer phantoms mimicking the brain and muscle and bilayer phantoms consisting of muscle and brain layers were prepared. The relative differences between the measured electrical conductivities of the monolayer brain and muscle phantoms and the true values determined by the 4-electrode method were both less than 10%. The relative differences between the measured and true values in the bilayer phantoms were less than 20% in both layers. The biological impedance measurement device that we developed was confirmed to be effective for impedance measurement in bilayer phantoms with different electrical impedances. To develop a device for the early diagnosis of breast diseases, the development of a multi-layer phantom and demonstration of the effectiveness of the device for its examination are necessary. If the device that we developed makes impedance measurement in breast tumors possible, it may be used as a new diagnostic modality for breast diseases. *J. Med. Invest.* 57 : 205-218, August, 2010

**Keywords :** *noninvasive, local tissue, electrical impedance tomography, measurement, breast diseases*

---

Received for publication January 4, 2010 ; accepted February 22, 2010.

Address correspondence and reprint requests to Kenji Okazaki, MD, Department of Thoracic, Endocrine Surgery and Oncology, Institute of Health Biosciences, the University of Tokushima Graduate School, Kuramoto-cho, Tokushima 770-8503, Japan and Fax : +81-88-633-7144.

## INTRODUCTION

Presently, imaging techniques such as radiography, ultrasonography, computed tomography (CT), and magnetic resonance imaging (MRI) are clinically

applied for the diagnosis of tumors. As is well known, radiography, ultrasonography, and CT represent information on the mass density distribution, and MRI represents information on the proton density distribution, as images. On the other hand, as the bioimpedance technique expresses the electrical characteristics of tissue structures of the body (1), it provides information essentially different from that generated by conventional imaging diagnostic techniques, i.e., the spatial distribution of electrical characteristics in the body, and there have been high expectations for the development of devices using this technique (2). The application of bioimpedance information to the measurement of the cardiac output, respiration, and body composition has long been attempted (3), but its precision has not reached a practical level. Morimoto et al. (4-6) confirmed differences in the impedance values between benign and malignant mammary gland tumors by measuring electrical impedance in the breast using the needle electrode method. This result suggests that quantitative judgment of whether a breast lesion is benign or malignant is possible employing the bioimpedance method, and that earlier and more accurate tissue diagnosis can be made by its combination with conventional imaging techniques. However, on measuring the electrical impedance of a tumor, the use of a needle electrode is invasive and clinically undesirable. For the application of electrical impedance information on tumors to the clinical diagnosis, the development of a device that can measure the electrical impedance of tumors noninvasively using skin-surface electrodes is required.

The objective of this study was to develop a measurement device using divided electrodes with guard electrodes proposed by Yasuno, Zhao et al. (7-9), and to validate its effectiveness using bioequivalent phantoms. For this purpose, we prepared an electrical impedance tomography (EIT) device and bioequivalent phantoms, measured the electrical characteristics of the phantoms, and performed validation tests using multi-layer bioequivalent phantoms.

## MATERIALS AND METHODS

### (1) Expression of electrical characteristics of biological tissues

The electrical characteristics of biological tissues may be expressed by either of the following 2 methods, 1) expression using electrically equivalent

circuits, 2) expression using the electric conductivity and permittivity. Biological tissues are made up of cell groups. Therefore, electrically equivalent circuits made up of one cell type can be expressed in a low-frequency zone as circuits consisting of the parameters extracellular resistance ( $R_e$ ), intracellular resistance ( $R_i$ ), and electrical capacitance of the cell membrane ( $C_m$ ) (1), as shown in Figure 1.  $R_e$ ,  $R_i$ , and  $C_m$  are the resistance component derived from extracellular fluid, resistance component derived from intracellular fluid, and capacity component derived from the cytoplasmic membranes, respectively. If the tissue structure is uniform, the entire tissue can be expressed by these equivalent circuits (Fig. 1).

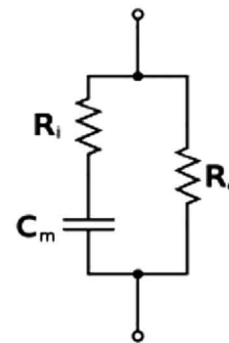


Figure 1 : Expression of biological tissue using electrical equivalent circuits (low-frequency range)

Using these electrically equivalent circuits, the bioelectric impedance  $Z$  is expressed by the following equation:  $Z = R_{\infty} - (R_{\infty} - R_e) / (1 - j\omega T)$ . Here,  $R_{\infty} = R_e R_i / (R_e + R_i)$  (total resistance of parallel resistors  $R_e$  and  $R_i$ ),  $T = C_m (R_e + R_i)$  (time constant), and  $\omega$  is each frequency. When the body is regarded as an electrical material, its electrical characteristics are expressed by the conductivity  $\sigma$  and permittivity  $\epsilon$ . The conductance per unit volume (unit cross-sectional area  $\times$  unit length)  $G (=1/z)$  [S/m] is expressed by the following equation:  $G = \sigma + j\omega\epsilon$ . Since there is no cell structure in a biological phantom, its electrical characteristics can be expressed by  $G$ . In experiments using bioequivalent phantoms in this study, the electrical characteristics of the phantoms were expressed using the conductivity and permittivity. These two expressions are interchangeable. If they are interchanged, the conductivity  $\sigma$  and permittivity  $\epsilon$  are usually functions of the frequency  $\omega$ . In the low frequency range of about 1 [kHz] discussed in this paper,  $\epsilon$  is negligible, only  $\sigma$  must be considered, and the value of  $\sigma$  can be regarded as a constant not dependent on the frequency.

(2) Measurement rationale

Figure 2 shows the arrangement of electrodes for the measurement of the bioelectric impedance. The divided electrodes with guard electrodes are composed of electric current and voltage electrodes. The same voltage  $v_i$  (1 [V]) is applied to the electric current electrodes placed outside (3 electrodes here), and the electric current  $i=(i_1, i_2, i_3)$  is applied to the body between the ground electrodes (potential : 0 [V]) arranged outside on the other side. Also, the voltage between electrodes  $v=(v_1, v_2, v_3)$  is measured with the 4 voltage electrodes placed between the electric current electrodes arranged on both ends. The current from the electric current electrode  $i=(i_1, i_2, i_3)$  flows in the body under the electrode, but it not only flows through the cross-section  $S$  beneath the electrode, but also spreads in a manner dependent on the 3-dimensional structure of the body. Therefore, the observed electrical impedance reflects the electrical characteristics of all body tissues as well as the cross-section  $S$  of the body beneath the electrode. For the bioimpedance to reflect the electrical characteristics of the cross-section of the body beneath the electrode alone, the electric current from the current electrode must be trapped in this cross-section.

The guard electrodes proposed by Yasuno and

Zhao et al. control the 3-dimensional diffusion of the electric current sent from the electric current electrodes through a 2-dimensional cross-section and substitute distribution equivalent circuits for the electrical characteristics of the 2-dimensional cross-section. The diffusion of the electric current is controlled within a 2-dimensional cross-section, as shown by the green part in Figure 2. Since guard electrodes are used for this purpose, and since the same voltage as the electric current electrodes is applied to them, diffusion of the electric current from the electric current electrodes can be prevented (7-9).

In this study, phantoms were used instead of the living body to experimentally examine the effectiveness of the proposed method. The electrical characteristics of a bioequivalent phantom can be expressed using the conductivity  $\sigma$  in a low frequency range. The method to estimate the distribution of the conductivity in cross-section  $S$  from the electric current  $i=(i_1, i_2, i_3)$  and voltage  $v=(v_1, v_2, v_3)$  measured using the measurement circuits in Figure 2 is outlined as follows : Here the voltage applied to the electric current electrode  $V_i$  is a sine curve alternating current with an amplitude of 1 [V] and a frequency of 1 [kHz]. From the electric current passing each electric current electrode  $i=(i_1, i_2, i_3)$  and the voltage between the voltage measurement

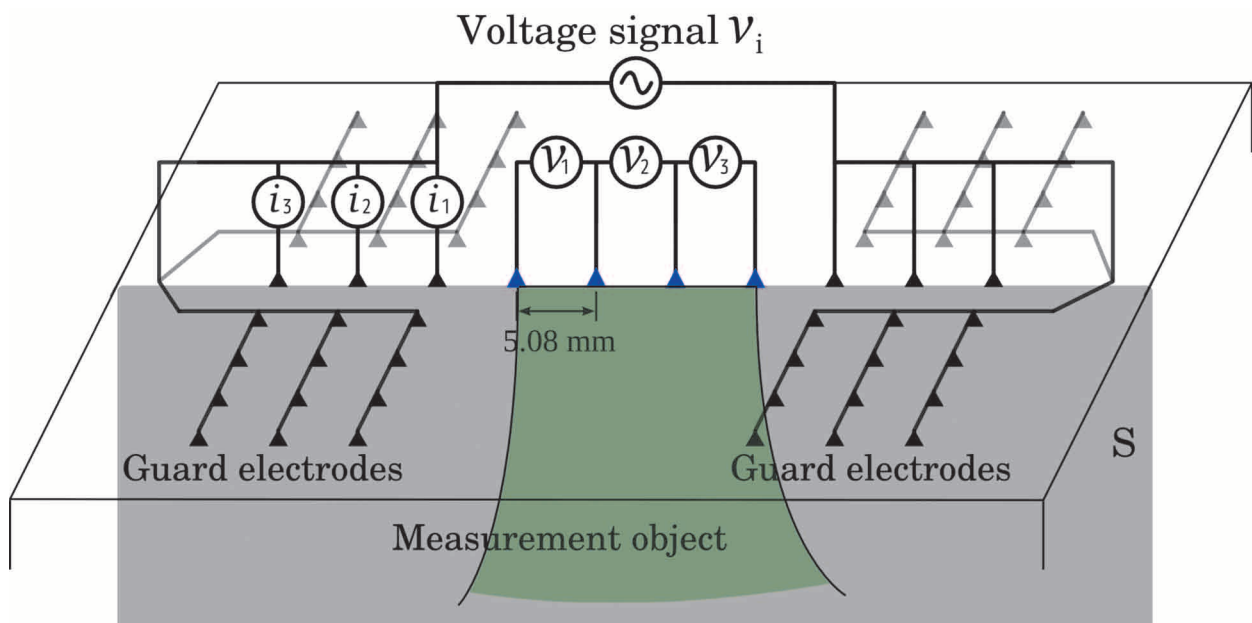


Figure 2 : Electrode arrangement for impedance measurement

The device consists of divided and guard electrodes. Because of the effect of the guard electrodes, the electric current that has passed from the electric current electrode is controlled within a 2-dimensional cross-section. The green area is the measurement area. The light black area is the cross-section  $S$  beneath the electrode.

electrodes  $\mathbf{v}=(v_1, v_2, v_3)$ , 9 resistances  $R_{nm}=v_n/i_m$  ( $n, m=1\sim 3$ ) can be determined, and they are expressed as  $\mathbf{R}=(R_{11}, R_{12}, \dots, R_{33})$ .

The structure of the cross-section of the phantom was converted to a model using computer software, and  $\mathbf{R}$  was calculated by numerical analysis using this model. This method is outlined as follows: The distribution of the conductivity  $\sigma$  [S/m] in the cross-section of interest of biological tissue (x-y 2-dimensional plane) is assumed to be  $\sigma(x,y)$ . At this time, the voltage distribution in this biological tissue cross-section  $v(x,y)$  can be calculated as the solution of the equation of Laplace.  $\partial/\partial x (\sigma(x,y) \partial v(x,y)/\partial x) + \partial/\partial y (\sigma(x,y) \partial v(x,y)/\partial y) = 0$  The electric current  $\mathbf{i}=(i_1, i_2, i_3)$  and voltage  $\mathbf{v}=(v_1, v_2, v_3)$  are determined by numerically solving the above equation using the boundary condition in which the voltage of the electric current electrode  $v_i=1$  [V], and the resistance  $\mathbf{R}=(R_{11}, R_{12}, \dots, R_{33})$  is calculated. This resistance is a function of  $\sigma(x,y)$ . To perform this calculation, the 2-dimensional cross-section is divided into a lattice pattern, and the solution is calculated using a matrix obtained by making the above equation of Laplace discrete. Here, if the resistance  $\mathbf{R}$  obtained by model analysis is designated as  $\mathbf{R}_m$ , and the resistance determined by the measurement experiment as  $\mathbf{R}_d$  (fixed value), the square error  $\varepsilon^2=||\mathbf{R}_m-\mathbf{R}_d||^2$  is a function of  $\sigma(x,y)$ . Therefore, the relationship can be expressed as  $\varepsilon^2=\mathbf{F}\{\sigma(x,y)\}$ . By performing a converging calculation of  $\sigma(x,y)$  that minimizes this error function  $\mathbf{F}$  by

the steepest descent method, the conductivity distribution in the cross-section of interest in a biological phantom can be estimated.

The bioequivalent phantoms used in this study had monolayer and bilayer structures, and  $\sigma(x,y)=\sigma_1$  in the monolayer phantoms and was an unknown quantity. In the bilayer phantoms, the conductivities of the two layers  $\sigma_1$  and  $\sigma_2$  were 2 unknown quantities.

### (3) Method for the measurement of conductivity (true value)

The conductivity of a material was measured using an impedance measurement device, and the intrinsic value of the material was regarded as the true value. It was necessary to examine the precision of the measurement device by regarding the difference between the true and observed values as an error. The true value was measured employing the four-electrode method (1), which is a standard method to determine the conductivity of materials. In this study, the conductivity (true value) was determined by the method shown in the diagram of Figure 3. A phantom with a volume of ABH [mm<sup>3</sup>] was sandwiched between 2 stainless steel plates and connected to a source of 1 kHz alternating current. The electric current passing through phantom I was calculated as  $I=V_1/R$  from the voltage  $V_1$  that appears on both ends of the resistor R connected in series with the phantom. Also,  $V_2$  was determined, using 2 electrodes for voltage measurement placed

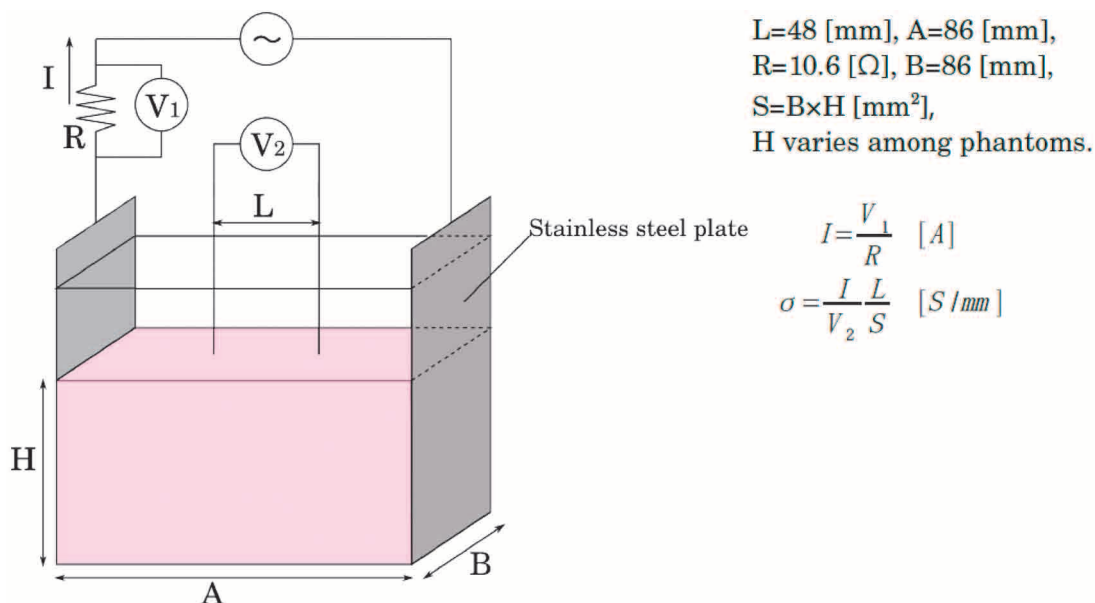


Figure 3 : Diagram of a measurement device based on the 4-electrode method

at a distance of  $L$  [m]. The method for conductivity measurement in the phantom can be expressed as equations  $I=V_1/R[A]$  and  $\sigma=I/V_2 \times L/S$  [S/mm]. The conductivity of the phantom calculated by this method was regarded as the true value. In this study,  $L=48$  [mm],  $A=86$  [mm],  $B=86$  [mm],  $R=10.6$  [ $\Omega$ ], and  $S=B \times H$  [mm<sup>2</sup>], with  $H$  varying among the phantoms.

(4) Bioequivalent phantoms

1. Bioequivalent phantoms used in this study and the procedure for their preparation

Bioequivalent phantoms prepared at Ito Laboratory, Department of Medical System Engineering at Chiba University (15) were used. The materials were agar (Wako Pure Chemical Industries, Ltd.), sodium chloride (Wako Pure Chemical Industries, Ltd.), dehydroacetic acid sodium salt (Wako Pure Chemical Industries, Ltd.), polyethylene powder (SUMITOMO SEIKA CHEMICALS CO., LTD. Inabata Fine Tech & Co., Ltd.), and TX-151 (Oil Center Research Inc., LA, USA). Bioequivalent phantoms were prepared as described from [1] to [7] below :

[1] In a pan, ion exchange water (tap water can also be used), sodium chloride, boric acid, and agar were placed and mixed until the contents become homogeneous.

[2] The mixture was heated over a gas cooking stove. During heating, the contents must be stirred continuously to avoid burning the agar.

[3] After boiling the mixture, the flame was immediately extinguished. Caution is necessary, because the agar does not gel if heating is insufficient.

[4] TX-151 was sprinkled into the pan in several parts and stirred quickly until it became homogeneous. (The operator must wear a mask to avoid inhaling the powder.) Be careful not to let bubbles form in the mixture.

[5] Polyethylene powder was also sprinkled into the pan in several parts and stirred until the mixture became homogeneous.

[6] The mixture was poured into a mold, wrapped in plastic film to prevent the evaporation of moisture, and allowed to cool at room temperature for about a day.

[7] After the phantom was gelled, it was removed from the mold, wrapped in plastic film, and stored at room temperature.

Concerning steps [4] and [5], TX-151 and polyethylene powder may be mixed well in advance and added together to the solution.

2. Composition and lifespan of the phantoms

Tables 1 and 2 show the compositions, electrical characteristics, and lifespans of the bioequivalent phantoms used (15).

3. Phantoms used in the experiments

In this study, monolayer and bilayer muscle and brain phantoms  $86$  [mm] $\times$  $86$  [mm] $\times$  $H$  [mm] ( $H$  varies among phantoms) were prepared and used for the measurements. Figure 4 shows a figure of

Table 1 : The composition of tissue containing a high-density water-equivalent phantom and its electrical characteristics

	Brain phantom	Muscle phantom	
Conductivity	0.83 [S/m]	1.43 [S/m]	
Ion-exchange water	3,375 [g]		
Agar	104.6 [g]		Independence of shape maintenance
NaCl (basic quantity)	21.5 [g]	37.6 [g]	Adjustment of permittivity
Preservative	Reference to Table 2		
TX151*	57.1 [g]	84.4 [g]	Adhesive
Polyethylene powder	54.8 [g]	337.5 [g]	Adjustment of the rate of permittivity

\*Oil Center Research Inc., LA, USA

Table 2 : The lifespan of a phantom

	Quantity [g]	Increased quantity of NaCl [g]	Lifespan
Sorbic acid	0.2	1.8	2 weeks
Dehydroacetic acid Na	2.0	1.6	Over 1 month
Boric acid	39.4	1.8	3 weeks

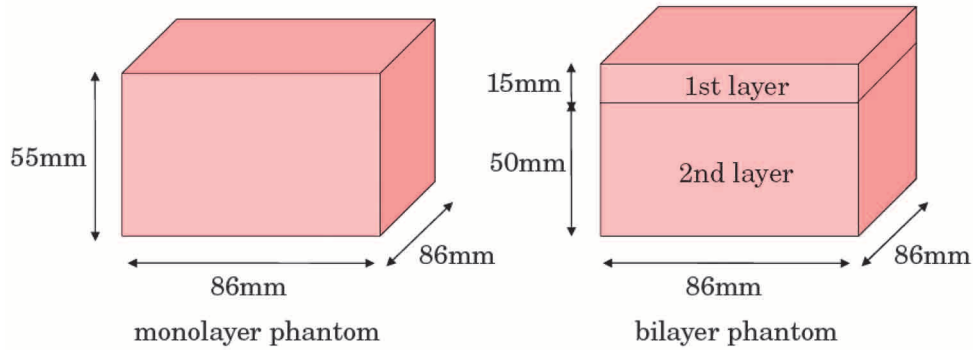


Figure 4 : A figure of monolayer phantom and of bilayer phantom

monolayer phantom and of bilayer phantom. Dehydroacetic acid Na salt was used as the preservative, and the phantoms were used in experiments within 1 month after their preparation.

(5) Experimental methods

1) Diagram and appearance of the measurement device

A 1 [kHz] alternating current was passed from

the impressed signal, and the voltage and electric current were measured using the voltage and current electrodes. The measurement area controlled within a 2-dimensional cross-section due to the effect of the guard electrodes is indicated in green (Fig. 5). Figure 6 is a block diagram of the measurement circuits of the measurement system (details are described in 3) Measurement Methods). Table 3 shows the instruments used, and Table 4

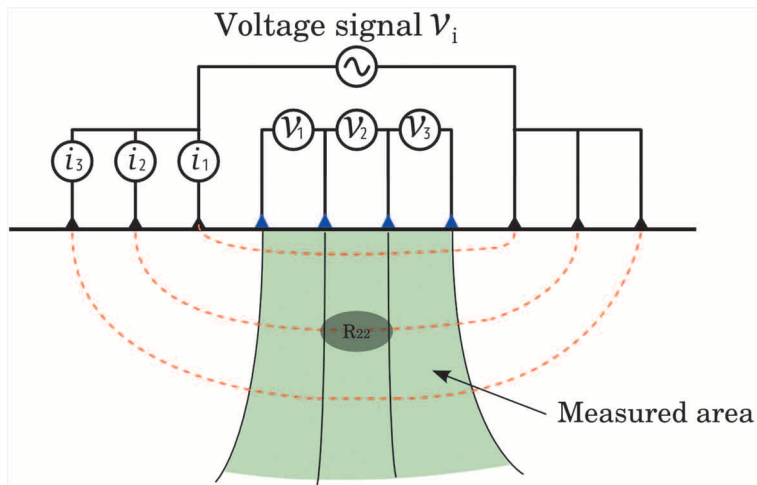


Figure 5 : Structure of the measurement device and measurement range  
 Red dotted lines : Electric current  
 Blue spots : Voltage electrodes  
 Black spots : Electric current electrodes  
 Black solid lines : Isovoltage lines  
 A 1 kHz alternating current was passed from the impressed signal, and the voltage and electric current were measured with the voltage and electric current electrodes. Because of the effect of the guard electrodes shown in Figure 2, the actual measurement area in Figure 5 was the 2-dimensional cross-section shown as the green area.

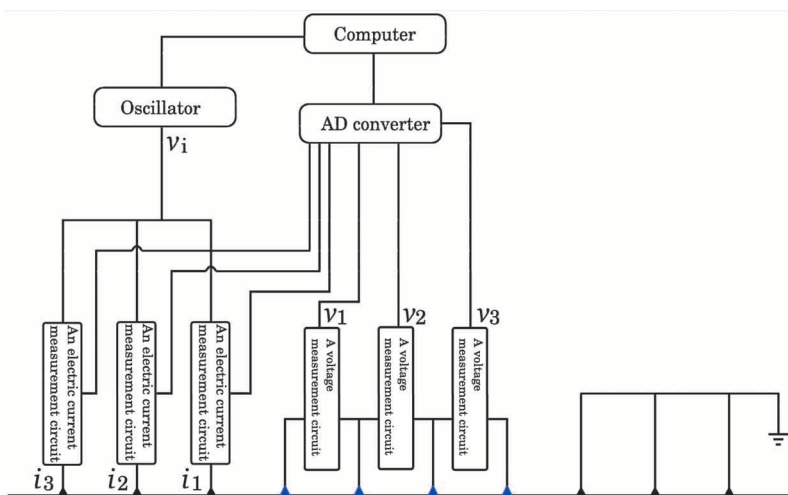


Figure 6 : Block diagram of the measurement system

Table 3 : Instruments used in the measurement system

Name	Manufacturer	Model	Specifications
Computer	DELL	PP07L	USB 2.0, with a PCMCIA port, Windows XP
Oscillator	NF	1915	Maximum output $\pm 10$ V, Frequency $\leq 2$ MHz, free waveform setting (4,096 points)
AD converter	Interface	CSI-360116	Resolution 12 bit, conversion time 1 $\mu$ S, voltage range $\pm 10$ V, maximum 16 ch

Table 4 : Specifications of the measurement system concerning the Measurable range and precision

	Measurable range <sup>*1</sup>	Precision of measurement <sup>*2</sup>
Electric current measurement circuits	$\pm 131 \mu$ A	$\pm 0.3\%$
Voltage difference measurement circuits	$\pm 1,310$ mV	$\pm 0.3\%$

\*1 : When  $\pm 15$  V was used as the power source

\*2 : Specifications of the products including the AD converter concerning the precision

shows the measurable range and precision according to the specifications of the measurement system. Figure 7 shows the appearance of a test model of our measurement device.

2) Diagram and appearance of measurement electrodes

Figure 8 shows the arrangement of measurement electrodes (bottom view), Figure 9 presents their

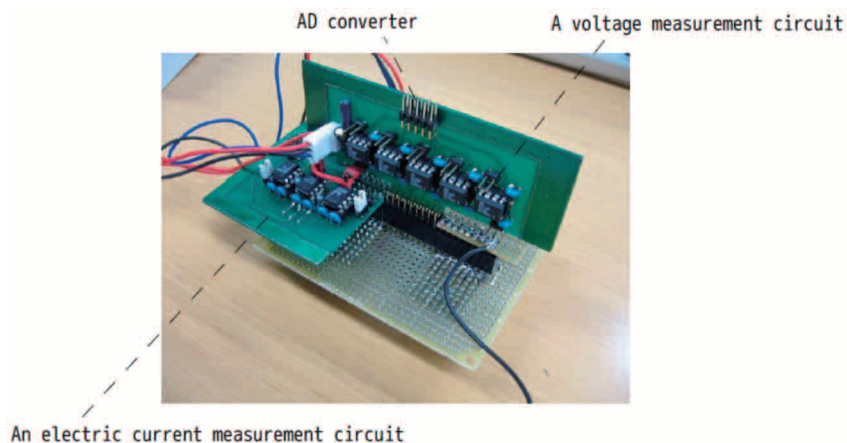


Figure 7 : Appearance of the measurement device  
The AD converter, electric current measurement circuits, and voltage measurement circuits are shown.

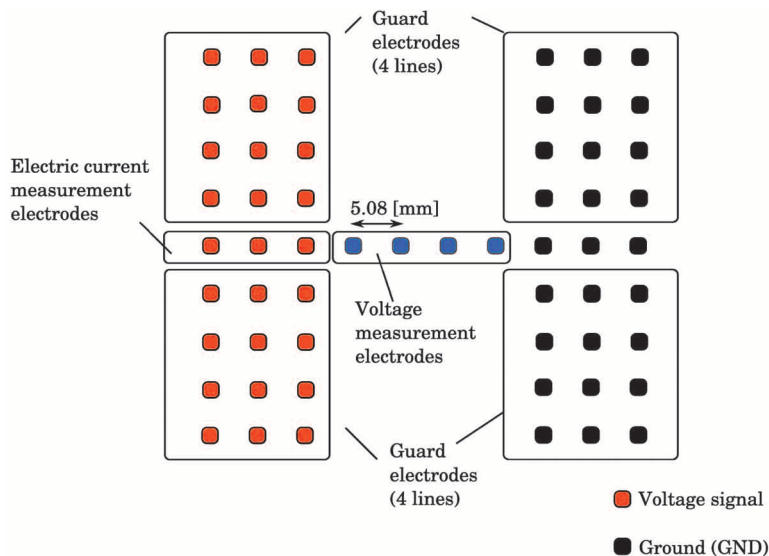


Figure 8 : Diagram of measurement electrodes (bottom view)

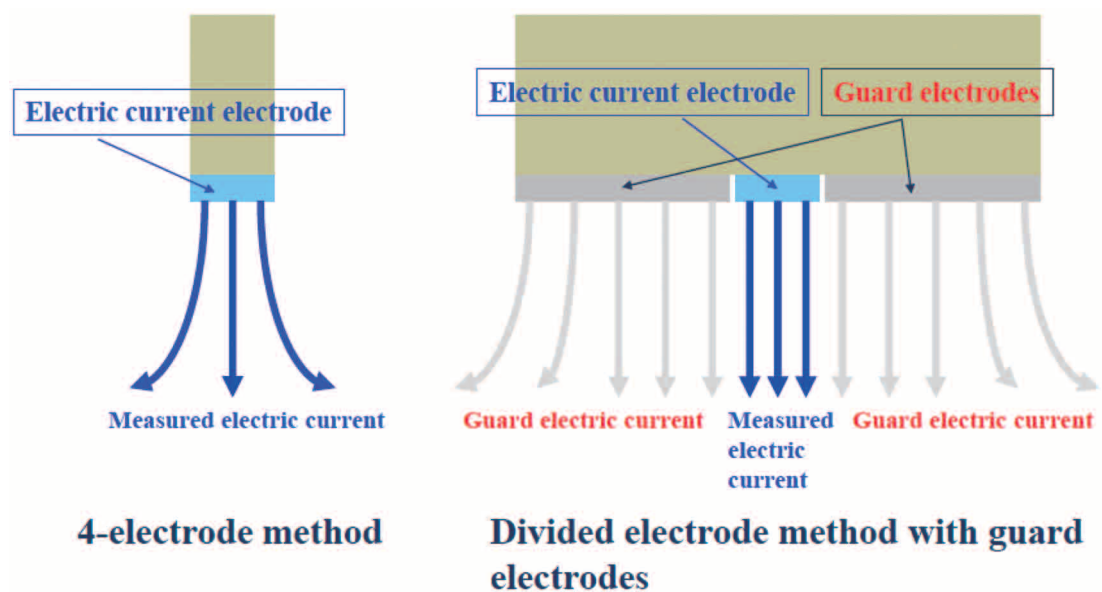


Figure 9 : Measurement electrodes (lateral view)

diagrams (lateral view), and Figure 10 shows their appearance. The electrodes used were JR-20Y, 1.9 [mm] in diameter (JAPAN SPRING PROBE CO., LTD.). They were arranged at intervals of 5.08 [mm], and current measuring, voltage measuring, guard, and ground electrodes were positioned as in Figure 8. Guard electrodes were placed at 4 sites (Fig. 8). Because of the effect of the guard electrodes, the actual flow of the electric current was controlled in a 2-dimensional cross-section. The ground electrodes were used to earth the system. Figure 9 shows diagrams of the measurement electrodes (lateral view). While the measured electric

current was diffused 3-dimensionally when using the 4-electrode method, it was controlled in a 2-dimensional cross-section and flowed linearly due to the effect of the guard electrodes in the divided electrode method.

### 3) Measurement method

The measurement was initiated as a computer signaled the oscillator, which generated a sine curve alternating current of 1 [kHz] and sent it to the electric current electrodes. The same voltage was simultaneously applied to the guard electrodes. Due to this voltage applied to the electric current electrodes, the electric current that flowed from each

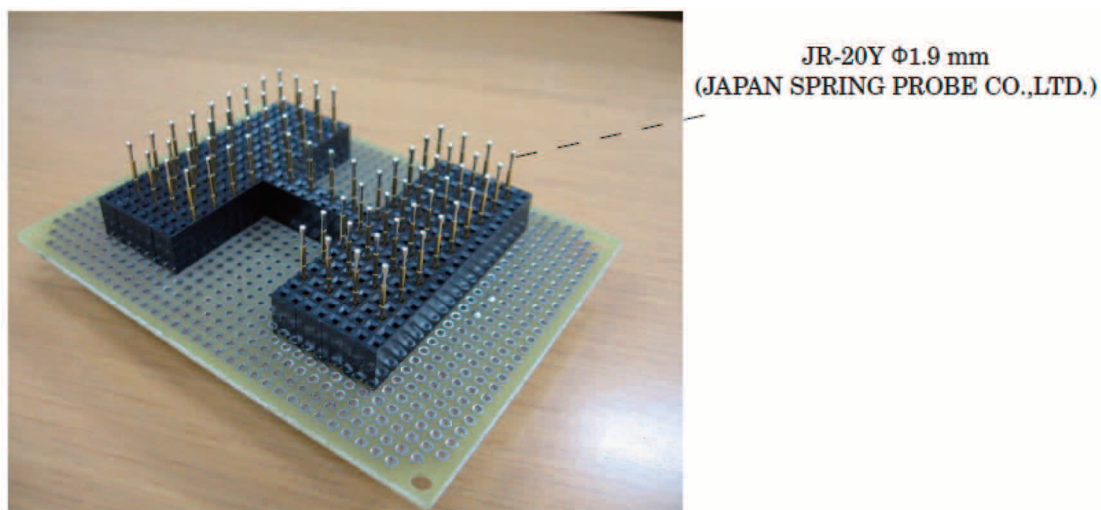


Figure 10 : Appearance of measurement electrodes  
JR-20Y spring electrodes 1.9 mm in diameter (JAPAN SPRING PROBE CO., LTD.) were arranged as above.

electric current electrode into the bioequivalent phantom was measured by the electric current measurement circuits. These measured signals were input into a computer through an AD converter. Also, due to the electric current flowing into the bioequivalent phantom, the voltage generated in the bioequivalent phantom was measured by the voltage electrodes and voltage measurement circuits, and their signals are also input into the computer through the AD converter. The signal amplitude was calculated from the electric current and voltage signal waveforms input into the computer, and the resistance  $\mathbf{R} = (R11, R12, \dots, R33)$  was calculated from these values (Fig. 6). Figure 11 shows a photograph of actual measurement. The measurement device was placed, an acryl resin board with a hole 1.8 [mm] in diameter was mounted on the

spring electrodes, and the phantom was placed in a manner that its ground surface was in even contact with the spring electrodes. A 1 kHz alternating current was passed, the voltage was measured, and the conductivity of the phantom was determined. Four lines of guard electrodes were used to control the 3-dimensional diffusion of the measured electric current within a 2-dimensional cross-section (7-9).

RESULTS

(1) Characteristics of the electrical responses of bioequivalent phantoms to a 1[kHz] low frequency alternating current

The bioequivalent phantoms used in this study were developed to examine the electrical characteristics of high-water-content tissues in a microwave frequency range (300-3,000 [MHz]). The impedance measurement device that we developed uses a 1 kHz low frequency alternating current power source, because evaluation of the characteristics of the bioequivalent phantoms in a low frequency range was necessary. We prepared muscle phantoms and studied changes in the conductivity with variations in the temperature and NaCl concentration. Figure 12 shows changes in the temperature of a bioequivalent phantom (muscle phantom). The conductivity changed only slightly from 1.5 to 1.6 [S/m] between 20 and 23 [°C]. Figure 13 shows

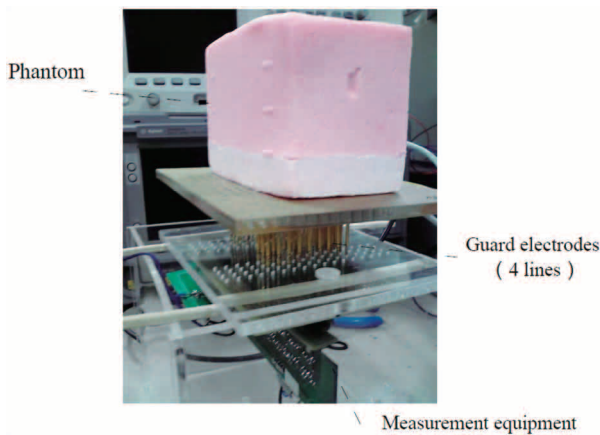


Figure 11 : A scene of actual measurement

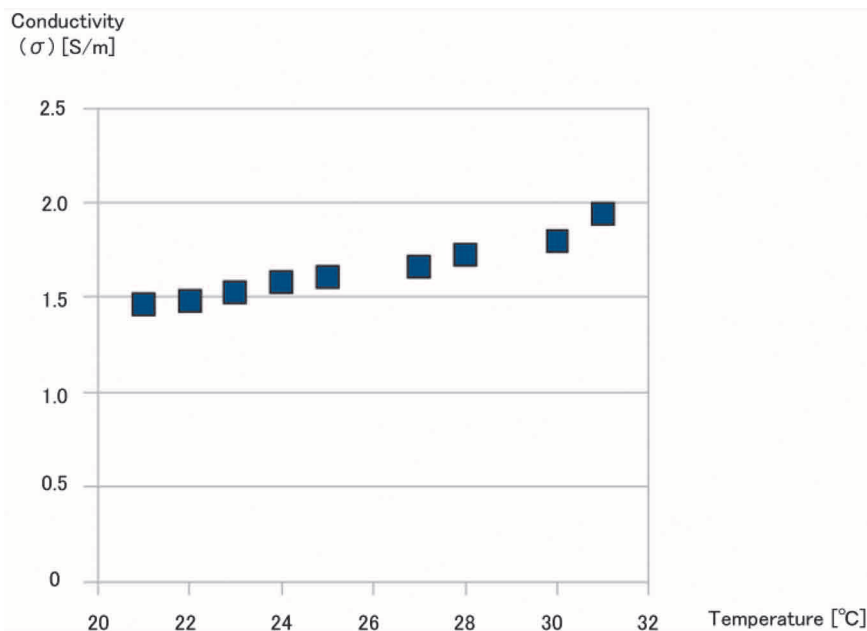


Figure 12 : Relationship between the conductivity and temperature changes in a bioequivalent phantom (muscle phantom)

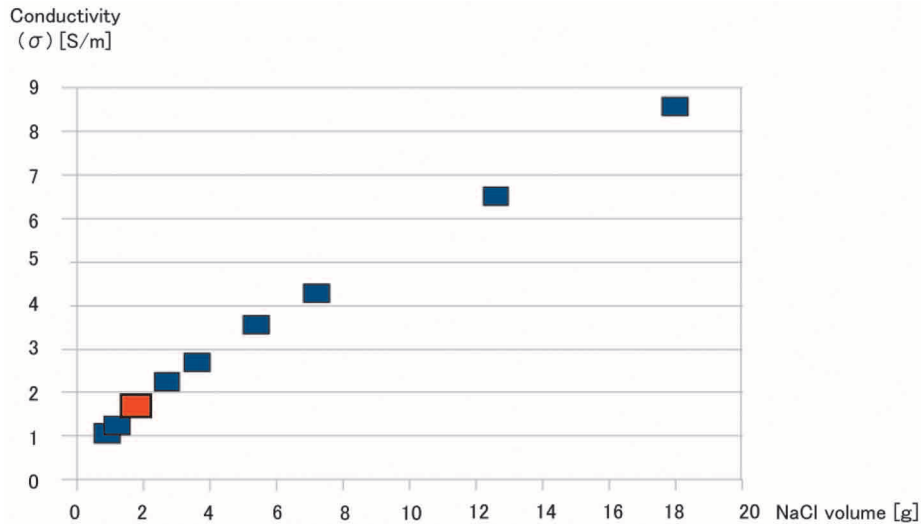


Figure 13 : Relationship between the conductivity and amount of NaCl

the relationship between the conductivity of a bio-equivalent phantom (muscle phantom) and NaCl concentration. The phantom was prepared using 1/20 of the amounts of the materials shown in Table 1. The red spot is the basal value shown in Table 1. The conductivity increased with the NaCl concentration. The conductivity of the monolayer muscle phantoms could also be adjusted by changing the NaCl concentration at a low frequency of 1 kHz, used in our impedance measurement device.

The characteristics of the conductivity of this phantom with a 1 kHz low frequency alternating current power source were shown to be similar to those in a microwave frequency range (300-3,000 [MHz]).

## (2) Measurement results

The results of conductivity measurements using the impedance measurement device were regarded as the estimated values, and those using the four-electrode method as the true values. The absolute value of the difference between the true and estimated values divided by the true value was defined as the relative difference (Relative difference =  $[\text{true value} - \text{estimated value}] \times 100 / \text{true value}$ ). All measurements were performed with an impressed signal of 0.5 [V<sub>p-p</sub>], 1 [kHz].

1) Results of measurements in monolayer phantoms (brain, muscle). The mean relative difference of 6 samples (monolayer brain phantoms) was  $5.75 \pm 2.92\%$ , being less than 10% (Table 5). The mean relative difference of 5 samples (monolayer muscle phantoms) was  $3.25 \pm 1.82\%$ , being less than 5% (Table 6).

Table 5 : Results of measurement of 6 monolayer brain phantoms

	True value (S/m)	Estimated value (S/m)	Relative difference (%)
1	0.896	0.810	9.60
2	0.778	0.713	8.33
3	0.778	0.762	2.12
4	0.741	0.766	3.36
5	0.740	0.708	4.52
6	0.755	0.708	6.57
Mean $\pm$ SD	$0.777 \pm 0.059$	$0.745 \pm 0.042$	$5.75 \pm 2.92$

Table 6 : Results of measurement of 5 monolayer muscle phantoms

	True value (S/m)	Estimated value (S/m)	Relative difference (%)
1	1.49	1.50	0.54
2	1.49	1.54	3.14
3	1.37	1.45	5.52
4	1.45	1.51	4.14
5	1.64	1.59	2.90
Mean $\pm$ SD	$1.488 \pm 0.098$	$1.518 \pm 0.052$	$3.25 \pm 1.82$

2) Results of measurements in bilayer phantoms : The first and second layers were the muscle and brain in 1 phantom and the brain and muscle, respectively, in the other. The estimated conductivity of the first muscle layer was 4.41%, and the relative difference of the second brain layer was 9.25%. The relative difference was less than 10% in each of the 2 layers (Table 7). The relative difference of the first brain layer was 18.4%, and that of the second muscle layer was 9.20%. The relative difference was less than 20% in each of the 2 layers (Table 8).

Table 7 : Results of measurement of a bilayer phantom (1st muscle layer, 2nd brain layer)

	True value (S/m)	Estimated value (S/m)	Relative difference (%)
1st layer muscle phantom	0.96	0.92	4.41
2nd layer brain phantom	0.79	0.87	9.25

Table 8 : Results of measurement of a bilayer phantom (1st brain layer, 2nd muscle layer)

	True value (S/m)	Estimated value (S/m)	Relative difference (%)
1st layer brain phantom	1.26	1.03	18.4
2nd layer muscle phantom	1.45	9.20	9.20

Although the results were from only 2 samples, the relative difference in each layer was less than 20%.

The relative differences between the true and measured values in the monolayer phantoms (brain, muscle) were less than 10%, indicating the satisfactory precision of the measurement device. The relative difference between the true and measured values was less than 20% in each layer of the bilayer phantoms, indicating the satisfactory precision of our measurement device also in bilayer phantoms.

## DISCUSSION

Yasuno, Zhao, et al. (7) established a method of regional electrical impedance tomography (EIT). Usually, an electric current generated from an electrode diffuses 3-dimensionally while it is transmitted. However, this 3-dimensional spread of the electric current generated from an electric current electrode can be controlled within a 2-dimensional cross-section through the use of divided electrodes with guard electrodes. By this method, the area of measurement can be restricted to a 2-dimensional cross-section, and the electrical characteristics of distribution equivalent circuits can be substituted for those in the cross-section. According to this theory, the electric impedance distribution in the cross-section of a tumor immediately below the divided electrodes is estimated using an algorithm for inverse problems by attaching divided electrodes and guard electrodes to the skin near the tumor as measurement electrodes. For the future clinical application of this newly developed technique of local EIT, its effectiveness must be validated by actual measurements using test devices prepared according to the theory. We performed experiments using

bioequivalent phantoms as the first step in basic research for this purpose. Such a measurement device is called impedance CT (2) or EIT and has been investigated by many researchers (10-13). Most of the studies on EIT have been conducted by attaching many electrodes to the skin of a part of the body (e.g., abdomen), and the electric impedance distribution of a cross-section of the body has been measured and represented as images (14). First, we prepared a prototype measurement device using divided electrodes with guard electrodes, and performed basic experiments using bioequivalent phantoms as the first step.

The characteristics of the bioequivalent phantoms used in this study were as follows : The human body can be divided into high-water-content tissues such as the muscle, brain, and viscera and low-water content tissues such as fat and bone, and their electrical characteristics (relative permittivity and conductivity) differ (16-22). The phantoms mimicked the electrical characteristics of high-water-content tissues in a microwave frequency range (300-3,000 [MHz]) and were characterized as follows :

[1] The raw materials are easy to acquire, and the phantoms can be prepared manually without special instruments.

[2] The phantoms can mimic the electrical characteristics of the living body over a wide frequency range with a single compositional ratio, and their electrical characteristics can be modified by changing the compositional ratio.

[3] The phantoms can be molded or carved into any desired shapes and show tight contact between separated surfaces.

Because of these characteristics, we judged that they were appropriate as materials for phantom experiments investigating the impedance measurement

device that we developed.

The relative difference in the results of measurements between the impedance and four-electrode methods was 10% or less in both the monolayer brain and muscle phantoms, indicating the validity of the measurement results. In the 2 bilayer phantoms consisting of 2 layers with different electrical resistances, the relative difference in each layer was less than 20%. We consider that our results demonstrated that bilayer phantoms with different electrical resistances can be examined with the bioimpedance measurement device that we developed. One problem with the examination of bilayer phantoms to be addressed in the future is the variability of the measurement results caused by small bubbles occurring at the interface between the layers and the consequent unevenness of the contact surface, which may grossly appear even. Thus, bilayer phantoms were suggested to be more difficult to prepare than monolayer phantoms.

In the past, Morimoto et al. (4, 5) intraoperatively measured the extracellular resistance ( $R_e$ ), the intracellular resistance ( $R_i$ ), and the electrical capacitance of the cell membrane ( $C_m$ ) in breast cancers, benign breast tumors (fibroadenomas), normal breast tissues, and adipose tissues at 10 [kHz] or below using needle electrodes among 54 patients (31 cases of breast cancer, 13 cases of fibroadenoma, and 10 cases of mastopathy). They found that  $R_e$  and  $R_i$  were significantly higher, and  $C_m$  was significantly lower, in breast cancer than in benign breast tumor (fibroadenoma). The mean  $R_e$  was  $1,445 \pm 586$  [ $\Omega$ ] in breast cancer,  $954 \pm 156$  [ $\Omega$ ] in fibroadenoma,  $772 \pm 203$  [ $\Omega$ ] in normal breast tissue, and  $6,044 \pm 3,388$  [ $\Omega$ ] in adipose tissue [6, 7]. When the parameters that we used for the evaluation of the experimental results were calculated using these data: Relative difference in  $R_e$  between fibroadenoma and normal breast tissue =  $(\text{Mean } R_e \text{ of fibroadenoma} - \text{mean } R_e \text{ of normal breast tissue}) \times 100 / \text{mean } R_e \text{ of normal breast tissue} = (954 - 772) \times 100 / 772 = 23.5\%$  Relative difference in  $R_e$  between breast cancer and normal breast tissue =  $(\text{Mean } R_e \text{ of breast cancer} - \text{mean } R_e \text{ of normal breast tissue}) \times 100 / \text{mean } R_e \text{ of normal breast tissue} = (1,445 - 772) \times 100 / 772 = 87.2\%$

The relative difference in  $R_e$  between fibroadenoma and normal breast tissue was 23.5%, and that between breast cancer and normal breast tissue was 87.2%. Therefore, if the relative difference of the electrical resistance measured with an impedance measurement device compared with the true value

in each of the 2 layers of a bilayer phantom with different electrical resistances is 20% or less, this technique is suggested to be clinically applicable for the diagnosis of breast cancer.

Ohmine, Morimoto, et al. (23) reported the results of conductivity measurement in the antebrachial muscle and adipose tissue in males and females. The conductivity was 0.40 [S/m] in the antebrachial region and 0.15 [S/m] in adipose tissue in males and 0.35 and 0.11 [S/m], respectively, in females. The absolute value of the difference between the muscle conductivity and adipose tissue conductivity divided by the muscle conductivity was defined as the relative difference (Relative difference =  $[|\text{muscle conductivity} - \text{adipose tissue conductivity}| \times 100] / \text{muscle conductivity}$ ). Relative difference between the adipose tissues and muscle conductivities in the male antebrachial region =  $(0.40 - 0.15) \times 100 / 0.40 = 62.5\%$  Relative difference between the adipose tissues and muscle conductivities in the female antebrachial region =  $(0.35 - 0.11) \times 100 / 0.35 = 68.6\%$  The relative difference between the antebrachial muscle and adipose tissue was 62.5% in males and 68.6% in females, being very high, exceeding 60%, in both genders. Since the relative difference was less than 20% in the results of measurements of the bilayer phantoms with different electrical resistances using the impedance measurement device that we developed, the technique was suggested to be applicable to the examination of bilayer structures with different conductivities such as the human antebrachium, consisting of adipose and muscle tissues.

For future clinical application, the preparation of small-size electrodes and a measurement device and their validation using multi-layer phantoms are necessary. Measurement of the living body, e.g., the anterior femoral region, in which the laminar structure is relatively clear, is also necessary. To develop a device for the early diagnosis of breast diseases, multi-layer phantoms must be developed, and the effectiveness of the device in the examination of such phantoms must be established. Yasuno et al. (24) reported a method to present data of  $R_e$ ,  $R_i$ , and  $C_m$  as images. This report suggests that the impedance of local tissues can be imaged using a measurement device incorporating divided electrodes with guard electrodes. Figure 14 shows an image prepared using data on  $R_e$ . If the impedance measurement device that we prepared is capable of impedance measurement in breast tumors, it may be developed as a new modality for the diagnosis of breast diseases.

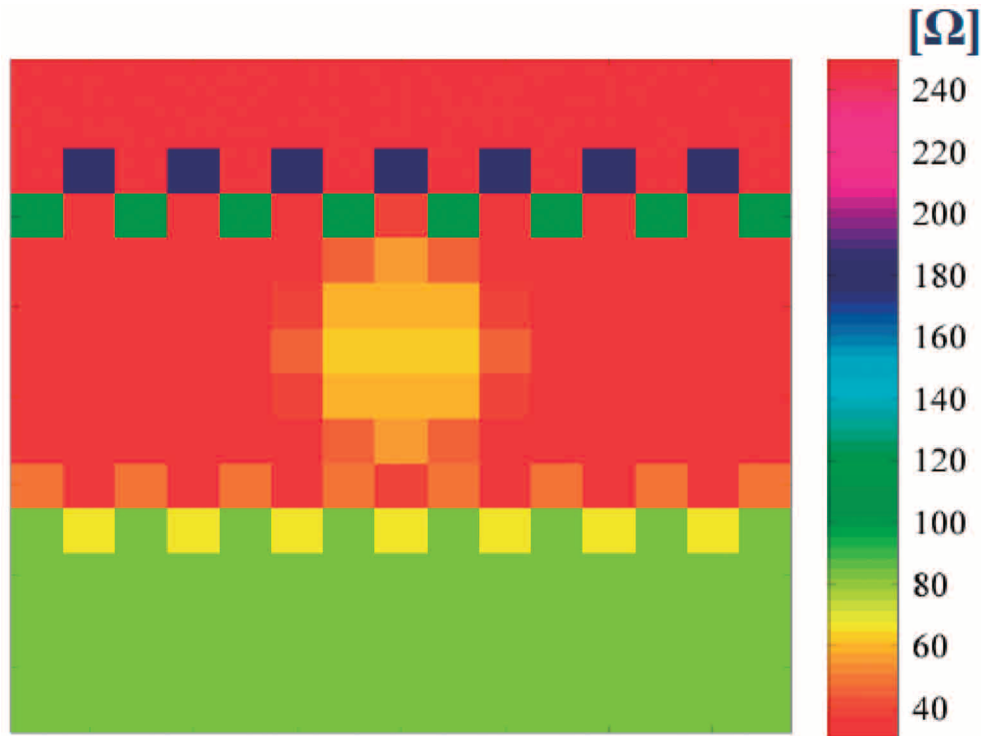


Figure 14 : An image derived from Re data

## REFERENCE

1. James JA, Martin AS : Methods of complex impedance measurements in biologic tissue. CRC 11(4) : 281-311, 1984
2. Sakamoto K : Impedance CT. Japanese Journal of Medical Electronics and Biological Engineering 8(8) : 49-56, 1994.
3. Baker LE : Application of the impedance technique to the respiratory system. IEEE Eng Med Biol Mag 8 : 50-52, 1989
4. Morimoto T, Kinouchi Y, Iritani T, Kimura S, Konishi Y, Mituyama N, Komaki K, Monden Y : Measurement of the electrical bio-impedance of breast tumors. Eur Surg Res 22(2) : 86-92, 1990
5. Morimoto T, Kimura S, Konoshi Y, Komaki K, Uyama T, Monden Y, Kiniuchi Y, Iritani T : A Study of the electrical bioimpedance of tumors. J Invest Surg 6(1) : 25-33, 1993
6. Ohmine Y, Morimoto T, Kinouchi Y, Iritani T, Takeuchi M, Monden Y : Noninvasive measurement of the electrical bioimpedance and its applications. Anicancer Res 20 : 1941-1946, 2000
7. Zhao X, Kinouchi Y, Iritani T, Morimoto T, Takeuchi M : Estimation of multi-layer tissue conductivities from non-invasively measured bioresistances using divided electrodes. IEICE Trans Inf Syst E85-D(6) : 1031-1038, 2002
8. Zhao X, Kinouchi Y, Yasuno E, Gao D, Iritani T, Morimoto T, Takeuchi M : A new non-invasive measurement of multi-layer tissue conductivity and structure using divided electrodes. IEEE Trans Biomed Eng 51(2) : 362-370, 2004
9. Yasuno E, Zhao X, Kinouchi Y, Morimoto T : Study on the estimation theory of space distribution for local tissue impedance CT. Transactions on the Japanese Society for Medical and Biological Eng 44(1) : 62-70, 2006(in Japanese).
10. David SH : Electrical impedance tomography. Institute of Physics Publishing, Bristol and Philadelphia, 2005
11. Yamamoto Y, Yamamoto T : Measurement of electrical bioimpedance and and its applications. Med Prog Technol 12 : 171-183, 1987
12. Ackmann JJ, Seitz MA : Methods of complex impedance measurements in biologic tissue. Crit Rev Biomed Eng 11 : 281-311, 1984
13. Alexander S, Aviram N, Zahava G : Electrical impedance scanning for the early detection of breast cancer in young women, Preliminary results of a multicenter prospective clinical trial. J Clin Oncolo 23 (12) : 2703-2715, 2005
14. Holder DS : Introduction to biomedical electrical impedance tomography, Electrical impedance

- tomography. Institute of Physics Publishing, Bristol and Philadelphia, 2005, pp.423-449
15. Furuya K, Hamada L, Ito K, Kasai H : A new muscle-equivalent phantom for SAR estimation. *IEICE Trans. Commun E78-B(6)* : 871-873, 1995
  16. Kritikos HN, Schwan AW : Hot spots generated in conducting spheres by electromagnetic waves and biological implications, *IEEE Trans BME19(1)* 53-58, 1972
  17. Kritikos HN, Schwan AW : Formation of hot spots in multilayer spheres, *IEEE Trans BME 23(3)* 168-172, 1976
  18. Johnson CC, Guy AW : Nonionizing electromagnetic wave effects in biological materials and systems, *IEEE l60(6)* 692-719, 1972
  19. Stucky MA, Stucky SS : Dielectric properties of biological substances-tabulated, *J Microwave Power 15(1)* 19-26, 1980
  20. Guy AW, Chou CK : Specific absorption rates of energy in man models exposed to cellular UHF mobile-antenna fields, *IEEE Trans. MTT 134 (6)* 671-680, 1986
  21. d'Inzeo G : Proposal for numerical canonical models in mobile communications, *Proc. COST 244 meeting on reference models for bioelectromagnetic test of modele communication systems 1-7*, 1994
  22. Gabriel C : Physical models for experimental EM dosimetry, Voxel phantom development, *Proc. international meeting held at the national radiological protection board, Clinton, UK*, 1995, pp. 46-53
  23. Ohmine Y, Morimoto T, Kinouchi Y, Iritani T, Takeuchi M, Haku M, Nishitani H : Basic study of new diagnostic modality according to non-invasive measurement of the electrical conductivity of tissues. *J Med Invest 51 (3, 4)* : 218-225, 2004
  24. Yasuno E, Kinouchi Y, Morimoto T, Ohmine Y : Estimation of space distribution for the local tissue impedance by using a divided electrode method. *IEE Japan IM-04-39* : 23-28, 2004(in Japanese).